Investigation of the Effect of Clay Nanoparticles on the Thermal Behavior of PLA Using a Heat Flux Rapid Scanning Rate Calorimeter

Prashanth Badrinarayanan[1,3], *Frank K. Ko*[2], *Chunhong Wang*[2], *Brian A. Richard*[3], *and Michael R. Kessler*[3,4]*

[1] *DuPont , Wilmington, DE,19803.*
[2] *Department of Materials Engineering, University of British Columbia, Vancouver, BC, V6T1Z4, Canada.*
[3]*Department of Materials Science and Engineering, Iowa State University, Ames, IA 50011*
[4]*School of Mechanical and Materials Engineering, Washington State University, Pullman, WA 99164.*

Abstract

In this work, the effect of clay nanoparticles on the glass transition and melting behavior of PLA was examined using a heat flux, rapid scanning rate calorimeter. The samples were prepared by electrospinning through incorporation of clay in the electrospinning solution, which facilitated composites with high filler loadings (15 – 25 wt.%). Dynamic heating scans at 500 ^{o}C/min were used to compare the effect of isothermal melt crystallization at various temperatures between 80 to 130 ^{o}C on the crystallization, melting, and glass transition behavior of PLA and PLA/clay nanocomposites. Incorporation of clay increased the crystallization kinetics of PLA only at lower loading levels. The incorporation of 15.3 wt. % clay resulted in only a slight reduction in the overall degree of crystallinity (w_c) in PLA, while a substantial reduction was observed with the incorporation of 25.0 wt. % clay. A significant reduction in the equilibrium melting temperature (T_m^0) was observed for nanocomposites containing 15.3 wt. % clay compared to the neat PLA fiber; however, the extent of reduction was mitigated when increasing the clay loading further to 25 wt. % . A similar trend was observed in the relationship between the glass transition temperature (T_g) and clay loading. Here, the PLA nanocomposites with 15.3 wt. % clay exhibited the lowest T_g values in both semicrystalline and amorphous samples. Elucidating the differences in thermal behavior and morphology of these nanocomposites as a function of clay loading is crucial for optimizing their physical and mechanical properties.

Keywords: A. Polymer Nanocomposites B. Thermal Properties D. Differential Scanning Calorimetry E. Electrospinning

***Corresponding author:** MichaelR.Kessler@wsu.edu

Introduction

Poly(lactic Acid) (PLA) is a semicrystalline polyester that can be derived from renewable sources, such as corn starch or sugar cane, and that exhibits thermomechanical properties comparable to petroleum-based plastics such as poly(ethylene terephthalate) [1]. Several researchers examined the potential to tailor the thermal, mechanical, and barrier properties of PLA through the incorporation of functional nanoparticles such as carbon nanotubes [2,3,4], titanium dioxide [5], silica [6,7], and clay [8-19] Clay nanocomposites with either PLA or poly(L-lactic acid) (PLLA) matrices are the most widely examined systems because they are biodegradable and because the clay nanoparticles can facilitate dramatic improvements in thermal and mechanical properties, as discussed in recent review articles [20,21].

The effect of the clay on the thermal behavior of PLA/clay nanocomposites depends on the nature of the clay and its interaction with the matrix and also on the processing technique used for preparing the nanocomposites. PLA/clay nanocomposites are typically manufactured by either solution casting [13,14] or melt processing techniques [15-19] such as extrusion and compounding. Pluta [19] used melt compounding to disperse up to 3 wt. % of Cloisite 30B clay nanoparticles in PLA. Differential scanning calorimetry (DSC) of the samples prepared by this method revealed a decrease in the onset temperature of cold crystallization exotherms observed on heating, which was attributed to the nucleating effect of the clay particles. Krikorian and Pochan [12] conducted detailed studies of the effect of clay loading and miscibility on the thermal behavior of PLLA/clay nanocomposite films. They reported that the presence of less miscible, intercalated clay particles resulted in a nucleating effect during PLLA crystallization, whereas such an effect was not observed for more miscible, exfoliated clay particles [12]. The presence of clay generally reduced the degree of crystallinity in PLLA, and the extent of the reduction was higher for the more miscible, exfoliated clay nanoparticles. As newer and more advanced techniques for processing polymer nanocomposites with better dispersion and higher aspect ratios are developed, it is necessary to determine the thermal behavior of the nanocomposites prepared by these methods.

With PLA/clay nanocomposites being used in a wide range of applications, such as textiles, packaging, and polymer composites, understanding the effect of significant clay loadings on the thermal properties of these nanocomposites systems becomes crucial. The objective of this work is to characterize the thermal behavior of PLA/clay nanocomposites

prepared by electrospinning using a rapid scanning rate DSC (Project RHC, TA Instruments). The effect of isothermal melt crystallization for 60 minutes at temperatures between 80 °C and 130 °C on the thermal behavior of electrospun PLA nanocomposites was examined. In addition, the effect of isothermal melt crystallization at 100 °C for various periods from 30 to 180 min was also characterized. Following the first heating scan, the fibers obtained by electrospinning effectively coalesced together and no longer retained the individual fiber morphology. However, because the emphasis of this work was on understanding the effect of high clay loadings on the thermal behavior of the PLA matrix, and electrospinning was simply the method of choice for accomplishing high filler loadings, the loss of individual fiber morphology was not considered a limiting factor.

In this work, we employed heating and cooling rates of 500 ^{o}C/min in order to prevent crystallization or recrystallization during the dynamic heating scans. However, it should be noted that the RHC DSC used in this work facilitates heating rates up to 2000 ^{o}C/min and cooling rates of 750 ^{o}C/min, depending on the temperature range, as described in detail elsewhere [22]. Commercial DSCs with even higher cooling and heating rates (several thousand degrees per second) are also available [23]. However, such measurements also require correspondingly small sample masses (on the nanogram scale).

Methodology

Materials

PLA pellets were obtained from NatureWorks (Blair, NE, USA); they had a weight average molecular weight (M_w) of 145,000 g/mol and a number average molecular weight (M_n) of 125,000 g/mol based on GPC measurements (relative to polystyrene) and a density of 1.24g/cm^3. Chloroform ($CHCl_3$, Fisher Scientific, Pittsburgh, PA) and dimethyl formamide (DMF, Sigma-Aldrich, St Louis, MO) were used to dissolve the PLA. Cloisite 30B, which exhibits high affinity and miscibility with PLA, is a natural montmorillonite (MMT) modified with a quaternary ammonium salt and was kindly donated by Southern Clay Products (Gonzales, TX). Its dry particle size distribution was 10 % < 2 μm, 50 % < 6 μm, and 90 % < 13 μm. Polyvinylpyrrolidone (PVP, Sigma-Aldrich) was used as a processing aid to disperse the nanoclay in the PLA matrix.

Preparation of Nanocomposites

For the preparation of pristine PLA samples, the PLA pellets (10 wt.% in solution) were solubilized in a 3:1 mixture of $CHCl_3$ and DMF by stirring with 1000 rpm at room temperature. The $CHCl_3$/DMF solution was added slowly to achieve the desired solution composition. For the solutions containing nanoclay, the PLA pellets were first dissolved in $CHCl_3$/DMF solution. Subsequently, two different loadings of nanoclay (2 and 4 wt. % of the overall electrospinning solution) and the required amount of surfactant PVP (50 wt. % of the respective clay loading) were added. The ratio of clay with respect to other components in the electrospinning mix is provided in Table 1. In the following, the samples will be referred as 0, 15.3, and 25.0 wt. % clay on the basis of the overall loading in the nanocomposite. The clay particles were dispersed in the solution by ultrasonic mixing for three hours using a sonic probe (Sonicator 3000, Misonix Inc., Farmingdale, NY).

The nanocomposite samples for this study were prepared by electrospinning, a non-mechanical technique, using a nanofiber electrospinning unit by Kato Tech Co., Ltd. Japan. First, the polymer solution was filled in a 10 mL syringe. The syringe was then placed in a metering pump with a set flow rate of 0.37 mL/h. A voltage of 15 kV was applied to the tip of the needle. A metal screen collector covered with aluminum foil was centered vertically at a distance of 15 cm from the syringe tip. The nonwoven fibers were compiled in to a mat for further characterization.

Characterization

Scanning electron microscopy (SEM) was performed to characterize the morphology of the prepared fiber mats using a Hitachi scanning electron microscope, operating at 20 kV. The fiber mats were mounted directly onto aluminum specimen stubs with double-sided adhesive carbon tabs and coated with gold in a Denton Desk II sputter coating unit for approximately 30 s at 40 mA and 50 mTorr with a working distance of 15 mm. Transmission electron microscopy (TEM) was performed to characterize the nature of clay dispersion in the nanocomposites. The fiber mat was embedded in an epoxy resin that was cured by UV irradiation. A cross section of the fiber mat embedded in the fully cured epoxy was examined using a JEOL 2100 200 kV microscope. TGA measurements were performed using a Q500 TGA (TA Instruments) with a heating rate of 20 °C/min from room temperature to 600 ^{o}C under nitrogen.

Rapid Scanning Rate Calorimetry

The experiments in this work were conducted using a using a beta version rapid scanning calorimeter developed under project RHC by TA instruments (New Castle, DE). The ballistic heating capabilities of the RHC DSC are based on four quartz halogen lamps, while the fast cooling measurements are accomplished through rapid circulation of liquid nitrogen. Various components of the DSC, including the sample cell and the sample pans, were miniaturized in order to minimize the effect of thermal gradients during ballistic heating/cooling measurements. The diameter of the sample pan was 0.16 mm, which is almost ten times smaller than a typical DSC sample pan. More detailed information on the construction and design of this unique instrument can be found elsewhere [22]. The electrospun fiber mats were cut into 5 mm × 5 mm pieces, folded, and compacted to fit inside the sample pans of the RHC DSC. The mass of the samples ranged between 0.1 to 0.2 mg.

The samples were heated at 500 °C/min to 200 °C and held isothermally for 1 minute to completely melt the material and erase all prior thermal histories. The samples were then brought from the melt to the crystallization temperature, T_{iso}, at 500 °C/min and held isothermally. The effect of a given isothermal history was examined by immediately quenching the samples to –150 °C following the isothermal hold at 500 °C/min and then heating them back to 200 °C at 500 °C/min .

Temperature and heat flow calibrations were performed at 500 ^{o}C/min using an indium sample. The values were recorded in the TA instruments software to perform the appropriate corrections for any offset based on the reference values of indium. The cell resistance and capacitance were calibrated using two sapphire standards. Helium gas at a flow rate of 25 ml/min was used to purge the sample cell for all experiments.

Results and Discussion

The SEM images of PLA mats with and without clay nanoparticles are shown in Figure 1. The clay particles were incorporated inside the PLA fibers and the variation in fiber diameter provided a measure of particle dispersion. The coefficient of variation in fiber diameter increased from 23 % for the PLA fiber to 33 and 39 % for the 15.3 wt. % clay and 25.0 wt. % clay samples, respectively. The greater extent of variation in fiber diameter for the 25.0 wt. %

clay samples may be indicative of some agglomeration of the clay particles at the higher loading. As noted in the introduction, the fibers effectively coalesced after the first heating scan to 200 °C. Hence, the images shown in Figure 1 only demonstrate the nature of the as-prepared fibers and the level of clay dispersion obtained by the electrospinning process. The presence of mostly intercalated clay particles in the nanocomposites was confirmed by the TEM images shown in Figure 2 a and b, which show the presence of ordered stacks for both the 15.3 and the 25.0 wt. % clay samples. The XRD spectra of the PLA clay nanocomposites are compared to the spectrum of Cloisite 30B in Figure 3. A well-defined peak of Cloisite 30B at $2\theta = 19°$ was observed in both nanocomposites, which confirms the presence of ordered structures of Cloisite 30B in the nanocomposites. It should be noted that the peak corresponding to Cloisite 30B completely disappeared when exfoliated nanocomposites were prepared, see the work of Krikorian *et al*. [11]. The TGA curves of the neat PLA sample and the two nanocomposites are shown in Figure 4. The residual weight % for the nanocomposite samples were 17.3 and 24.6 %, respectively, which was in reasonable agreement with the expected loading in the composite. The slight differences between observed residual weight and expected value based on loading shown in Table 1 were attributed to the fact that PLA contributes a small residual weight (2.0 %) under nitrogen and to potential differences in dispersion.

The benefit of using rapid scanning rates for this study is illustrated in Figures 5a and b by a comparison between data obtained with conventional and rapid scanning calorimetry. The heat flow curves obtained by heating the as-prepared neat PLA using a slow heating rate of 20 °C/min is shown in Figure 5a (1^{st} heating scan). Upon heating the sample above 50 °C, the onset of the glass transition caused a step change in the heat flow. The sharp peak accompanying the glass transition was associated with enthalpy relaxation, which was immediately followed by a crystallization exotherm, suggesting that the sample was not completely crystallized during the electrospinning process. Further heating led to a melting endotherm between 135 and 145 °C, after which the sample was completely transformed to a melt. Following the first heating scan, the melted sample was immediately cooled at 20 ^{o}C/min back to the glassy state and reheated at 20 ^{o}C/min, as shown in Figure 5a (2^{nd} heating scan). The second heating scan revealed a glass transition in the same temperature range as during the first heating scan; however, the significant enthalpy relaxation peak that was observed in the first heating scan did not occur. It should be noted that the enthalpy relaxation peak is usually minimal or absent in DSC measurements

during the second heating when the heating rate is identical to the preceding cooling rate. A small melt endotherm was observed on heating beyond 140 °C, which suggests that some crystals had formed during the cooling scan at 20 ^{o}C/min.

The heat flow curve observed on heating the as-prepared neat PLA at 500 °C/min using RHC DSC is shown in Figure 5b (1st heating scan). The material exhibited a glass transition accompanied by a pronounced enthalpy relaxation peak. Unlike during the 1st heating scan at 20 ^{o}C/min, no crystallization exotherm was observed following the low temperature melting endotherm for the first heating scan at 500 °C/min. Further heating led to an endothermic melting transition between 135 and 145 °C, after which the sample was completely transformed to a melt. Following the first heating scan at 500 °C/min, the sample was quenched at 500 ^{o}C/min to –150 °C and heated back at 500 °C/min, as shown in Figure 5b (2nd heating scan). During the second heating scan, only a step change in heat flow caused by the glass transition was observed. In addition, no crystallization exotherm or melting endotherm was observed over the entire temperature range, which indicates that this thermal history (cooling and reheating at 500 °C/min) was sufficient to ensure that crystallization did not occur during the measurement scan. The absence of a crystallization exotherm, which overlaps with the enthalpy relaxation peak, facilitated a more precise estimate of the crystallinity of the as-prepared material in the first heating scan using rapid scanning calorimetry. Such an estimate would be a challenge even with techniques such as modulated DSC, which can separate thermal events that are either reversing or non-reversing during the modulation cycles, because both enthalpy relaxation and cold crystallization would be observed in the non-reversing signal.

Figures 6a through c show the melting endotherms observed during the second heating scan at 500 °C/min for the neat PLA and the PLA/clay nanocomposites following isothermal melt crystallization at various temperatures between 80 to 130 °C for 60 minutes. The effect of T_{iso} on the peak temperature (T_m) of the melting endotherm for PLA with and without nanoclay is shown in Figure 7. Two melting peak temperatures were reported for the nanocomposite samples at T_{iso} = 80 °C caused by the occurrence of multiple melting behaviors.

The neat PLA sample did not exhibit multiple melting behaviors for the thermal histories employed in this work; however, the occurrence of multiple melting behaviors in PLA has been reported following certain thermal histories [24-30]. The determination of the origin for the multiple melting behaviors in PLA and other semicrystalline polymers drives the extensive,

ongoing debate in the literature [31-37]. Various explanations have been suggested for the low temperature endotherm, including melt-recrystallization processes of the crystal lamella, the melting of thinner crystal lamella, devitrification or relaxation of the rigid amorphous phase, and more recently for PLLA, a phase transition from the α' to the α phase [26, 28]. For values of T_{iso} greater than 80 °C, the values of T_m increased with increasing T_{iso}, as expected. The values of T_m were slightly reduced for the 15.3 wt. % clay nanocomposite compared to neat PLA and the 25.0 wt. % clay nanocomposite. The melting temperature data may be used to determine the equilibrium melting point (T_m^0) using the Hoffman Weeks approach [38], which is still widely used because of its simplicity, although some limitations and potential modifications have also been reported [39]. In the simplest form of this method, T_m^0 is determined as the point of intersection between the T_m *vs.* T_{iso} curve with a straight line that assumes $T_m = T_{iso}$, as shown in the inset of Figure 7. The value of T_m^0 for neat PLA was determined as 178.5 °C, while the values of T_m^0 for the 15.3 wt. % clay and 25.0 wt.% clay samples were determined as 166.6 °C and 171.8 °C, respectively.

The relationships between T_{iso} and the degree of crystallinity (w_c) for neat PLA and the nanocomposites following isothermal melt crystallization for 60 minutes are compared in Figure 8. For DSC measurements of polymer nanocomposites, the value of w_c may be estimated as shown in Equation 1 below:

$$w_c = \frac{\Delta H_m}{x \ \Delta H_m^{\ 0}} \qquad (1)$$

where x is the weight fraction of the PLA polymer phase and ΔH_m^0 is the enthalpy of melting of 100 % crystalline PLA, which is reported to be 91 J/g [40]. It should be noted that Equation 1 excludes any potential contribution from either the inorganic filler or the PVP phase towards the melting endotherm of PLA. PVP, which is incorporated as a processing aid, is a completely amorphous polymer, with a T_g that is above the melting range of the PLA used in this work [41]. Furthermore, as shown by prior work [42], blends of PLA and PVP are completely immiscible and the PVP phase contributes neither to the glass transition nor to the melting endotherm of PLA. In this work, a separate T_g for the PVP was not observed beyond the melting temperature range, which is consistent with prior work [42] for DL-PLA/PVP blends, where a separate T_g for PVP was observable only at PVP concentrations higher than 30 wt. %. Considering the large

surface area of the nanoclay and the lower loading level of PVP, the effect of the clay is clearly more dominant.

The determination of ΔH_m was performed consistently for all samples by integrating the entire area from the onset to the end of the melting process for the curves shown in Figures 6a through c. For T_{iso} = 80 °C, the value of w_c increased from zero for neat PLA to 0.32 for the 15.3 wt. % clay samples. The lack of melting endotherm following isothermal melt crystallization at 80 °C for 60 minutes for neat PLA was attributed to the slow crystallization rate of PLA at this particular temperature; the incorporation of clay increased the rate of crystal formation because of the nucleating effect [12,19] of the clay nanoparticles. However, the average value of w_c for the 25.0 wt. % clay sample following isothermal melt crystallization at 80 °C for 60 minutes was only 0.08. This trend of decreasing crystallization kinetics on increasing clay loadings beyond a certain level was also reported in the literature [43] and was attributed to an increase in constraints imposed on the polymer chains by the presence of several clay particles in close proximity, inhibiting their incorporation into the crystal lamella.

The relationship between w_c and T_{iso} was also different for neat PLA and the nanocomposites. In the case of neat PLA, the crystallization kinetics was slowest at lower (80, 90 °C) or higher (130 °C) T_{iso}s , which led to a bell shaped curve for w_c *vs.* T_{iso}. For the 15.3 wt. % clay nanocomposite, the expedited kinetics caused by the nucleating effect of the clay nanoparticles ensured that crystallization was complete at all temperatures from 80 – 120 °C and w_c remained invariant with T_{iso} in this temperature range; when T_{iso} was subsequently raised to 130 ^{o}C, the crystallization rate decreased. For the 25.0 wt. % clay nanocomposite, the increase in kinetics was lower compared to the 15.3 wt. % clay sample, with w_c increasing with T_{iso} up to 90 °C and remaining constant up to 120 °C, before it eventually decreased at 130 °C. The value of w_c for the 15.3 wt. % clay nanocomposite was lower than the corresponding value for 25.0 wt. % clay nanocomposite at T_{iso} =130 °C. This can be explained by the lower T_m and the proximity of T_m to T_{iso} for the 15.3 wt. % clay nanocomposite.

Figure 8 shows that a crystallization period of 60 min may be sufficient for complete crystallization only at certain temperatures, especially for neat PLA. Therefore, the degree of crystallinity as a function of crystallization period was compared for neat PLA and the two PLA/clay nanocomposites to conclusively demonstrate the effect of clay loading on the overall degree of crystallinity. Such a comparison is shown in Figure 9 following isothermal melt

crystallization for various durations from 30 to 180 min at T_{iso} =100 °C. For all three samples, the values of w_c did not change with time after a crystallization period of 90 min, indicating completion of crystallization at this duration for T_{iso} = 100 ^{o}C. Upon comparing the effect of clay loading on crystallinity for crystallization periods longer than or equal to 90 min, the value of w_c is found to be slightly lower for the 15.3 wt. % clay nanocomposite when compared to neat PLA. However, the most prominent reduction in crystallinity was observed for the 25.0 wt. % clay nanocomposite. This decrease in overall crystallinity can be attributed to the increase in nucleation sites, which initially promotes the crystallization kinetics, but ultimately hinders the incorporation of the polymer chains in the crystal lamella [12].

While incorporation of clay had a clear effect on the crystalline phase of PLA, the effect on the amorphous domains was determined by comparing of the T_gs for samples with various clay loadings. The T_g of the 15.3 wt.% clay sample was significantly lower than the T_g of neat PLA , as shown in Figure 10. However, the T_g of 25.0 wt. % clay was higher than that of the 15.3 wt. % clay sample. The value of T_g was determined by the fictive temperature method [44] as the point of intersection of tangents drawn from the glassy and liquid regions of the integrated heat flow data. In order to determine the effect of clay loading and crystallinity on the amorphous glass transition of PLA and its nanocomposites, T_g was also measured after the samples had been heated at a rate of 500 ^{o}C/min followed by cooling of the sample from the melt at a rate of 500 ^{o}C/min to render the samples completely amorphous. For all three samples, the T_g values were higher for semicrystalline PLA samples compared to amorphous samples. However, the relationship between T_g and clay loading for semicrystalline and completely amorphous samples was similar, as shown in Figure 10. Here, the values of T_g for 15.3 wt. % clay samples were significantly lower than the values obtained for PLA and the 25.0 wt. % clay nanocomposite samples. The 15.3 wt. % clay sample exhibited not only a lower T_g but also a lower T_m^0, compared to PLA and 25.0 wt. % clay samples. These differences cannot be explained by differences in PVP concentration, because PVP is immiscible with PLA and has not been reported to cause any change in the T_g of amorphous PLA, even at very high loadings [42, 45].

A potential reason for the decrease in T_g and T_m^0 for the better dispersed 15.3 wt. % clay system could be the plasticizing effect of the quaternary ammonium surfactants in Closite 30B, as reported in earlier work [46]. On the other hand, in the case of 25.0 wt. % clay samples, the

reinforcing effect of the clay nanoparticles might overcome the plasticizing effect, resulting in a higher value of T_g or T_m^0 compared to the 15.3 wt. % clay sample.

The results of our investigation demonstrated the differences in the crystallization, melting, and glass transition behavior of PLA/clay nanocomposites, not only as a consequence of clay loading but also caused by their thermal history. Because the thermal behavior of these nanocomposites directly impacts their processability and biodegradability, the identification of these differences is essential for the development of nanocomposites with optimum properties.

Conclusions

In this work, the thermal behavior of PLA and PLA/clay nanocomposites prepared by electrospinning was characterized using rapid scanning rate calorimetry. The effect of isothermal melt crystallization at various temperatures between 80 and 130 °C was characterized after heating at a rate of 500 °C/min. Following isothermal melt crystallization at 80 °C for 60 min, neat PLA did not exhibit a melting endotherm (i.e., $w_c = 0$), whereas the average value of w_c was 0.3 for the 15.3 wt. % clay sample, indicative of a nucleating effect of the incorporated clay. On the other hand, a further increase in clay loading to 25 wt.% lowered the kinetics at 80 °C compared to the 15.3 wt. % clay sample. For thermal histories during which crystallization was completed, the overall value of w_c decreased slightly with incorporation of 15.3 wt. % clay while a more significant reduction was observed with incorporation of 25.0 wt. % clay. The equilibrium melting point (T_m^0) of PLA decreased with incorporation of 15.3 wt. % clay, while the extent of reduction was mitigated with incorporation of 25.0 wt. % clay. A similar trend was observed for the glass transition behavior of PLA and PLA/clay composites with increasing clay loading. The T_g of both semicrystalline and amorphous PLA was reduced with incorporation of 15.3 wt. % clay, while incorporation of 25.0 wt. % clay did not result in a significant reduction. The origin for this surprising trend was not obvious, but a potential cause for the loss of thermal stability of the well dispersed PLA/15.3 wt. % clay samples may have been a plasticizing effect of surfactants present in the clay, which was overcome by the reinforcing effect of higher clay loadings.

Acknowledgements:

We acknowledge TA Instruments for providing the rapid scanning calorimeter used in this work, as a part of project RHC. Financial support by the Iowa Space Grant Consortium and by the

National Science Foundation through the CAREER program under Award No. 0954314 is gratefully acknowledged.

References

1. Auras R, Harte B, Selke S. Effect of water on the oxygen barrier properties of poly(ethylene terephthalate) and polylactide films. *Journal of Applied Polymer Science* 92, 1790-1803 (2004) DOI: 10.1002/app.20148
2. Moon SI, Jin F, Lee CJ, Tsutsumi S, Hyon SH. Novel carbon nanotube/poly(L-lactic acid) composites: their modulus, thermal stability, and electrical conductivity. *Macromolecular Symposia* 224, 287-295 (2005) DOI: 10.1002/masy.200550625
3. Xu JZ, Chen T, Yang CL, Li ZM, Mao YM, Zeng BQ, Hsiao BS. Isothermal Crystallization of Poly(L-lactide) Induced by Graphene Nanosheets and Carbon Nanotubes: A Comparative Study. *Macromolecules* 43, 5000-5008 (2010). DOI: 10.1021/ma100304n
4. Ramontja J, Sinha SS, Pillai SK, Luyt AS. High-performance carbon nanotube-reinforced bioplastic. *Macromolecular Materials and Engineering* 294, 839-846 (2009). DOI: 10.1002/mame.200900197
5. Fukuda N, Tsuji H. Physical properties and enzymatic hydrolysis of poly(L-lactide)–TiO2 composites. *Journal of Applied Polymer Science* 96, 190-199 (2005) DOI: 10.1002/app.21411
6. Zhang J, Lou J, Ilias S, Krishnamachari P, Yan J. Thermal properties of poly(lactic acid) fumed silica nanocomposites: Experiments and molecular dynamics simulations. *Polymer* 49, 2381-2396 (2008) DOI: 10.1016/j.polymer.2008.02.048
7. Yan S, Yin J, Yang J, Chen X. Structural characteristics and thermal properties of plasticized poly(l-lactide)-silica nanocomposites synthesized by sol–gel method. *Materials Letters* 61, 2683-2686 (2007) .
8. Ogata N, Jiminez G, Kawai H, Ogihara T. Structure and thermal/mechanical properties of poly(l-lactide)-clay blend. *Journal of Polymer Science, Part B: Polymer Physics* 35, 389-396 (1997) DOI: 10.1002/(SICI)1099-0488(19970130).
9. Paul MA, Michael A, Degee P, Henrist C, Rulmont A, Dubois P. New nanocomposite materials based on plasticized poly(L-lactide) and organo-modified montmorillonites: Thermal and morphological study. *Polymer*; 44, 443-450 (2002) DOI: 10.1016/S0032-3861(02)00778-4
10. Ray SS, Yamada K, Okamoto M, Ogami A, Ueda K. New Polylactide/Layered Silicate Nanocomposites. 3.High-Performance Biodegradable Materials. *Chemistry of Materials*; 15, 1456-1465 (2003) DOI: 10.1021/cm020953r
11. Krikorian V, Pochan DJ. Poly (L-Lactic Acid)/Layered Silicate Nanocomposite: Fabrication, Characterization, and Properties. *Chemistry of Materials*;15, 4317-4324 (2003) DOI: 10.1021/cm034369.
12. Krikorain V, Pochan DJ. Unusual Crystallization Behavior of Organoclay Reinforced Poly(L-lactic acid) Nanocomposites . *Macromolecules* 37:6480-6491 (2004) DOI: 10.1021/ma049283w
13. Jeszka JK, Pietrzak L, Pluta M, Boiteux G. Dielectric properties of polylactides and their nanocomposites with montmorillonite. *Journal of Non Crystalline Solids* 2010;356:818-821. DOI: 10.1016/j.jnoncrysol.2009.06.057.

14. Chang JH, An YU, Sur GS. Poly(lactic acid) nanocomposites with various organoclays. I. Thermomechanical properties, morphology, and gas permeability. *Journal of Polymer Science: Part B: Polymer Physics* 2003;41: 94-103. DOI: 10.1002/polb.10349
15. Ray SS, Yamada K, Okamoto M, Fujimoto Y, Ogami A, Ueda K. New polylactide/layered silicate nanocomposites. 5. Designing of materials with desired properties. *Polymer* 2003; 44: 6633-6646. DOI: 10.1016/j.polymer.2003.08.021
16. Jiang L, Zhang JW, Wolcott MP. Comparison of polylactide/nano-sized calcium carbonate and polylactide/montmorillonite composites: Reinforcing effects and toughening mechanisms. *Polymer* 2007;48:7632-7644. DOI: 10.1016/j.polymer.2007.11.001
17. Pluta M, Galeski A, Alexandre M, Paul MA, Dubois P. Polylactide/montmorillonite nanocomposites and microcomposites prepared by melt blending: Structure and some physical properties. *Journal of Appliedl Polymer Science* 2002;86: 1497-1506. DOI: 10.1002/app.11309
18. Pluta M. Morphology and properties of polylactide modified by thermal treatment, filling with layered silicates and plasticization. *Polymer* 2004;45:8239-8251. DOI: 10.1016/j.polymer.2004.09.057
19. Pluta M. Melt compounding of polylactide/organoclay: Structure and properties of nanocomposites. *Journal of Polymer Science Part B: Polymer Physics* 2006;44:3392-3405. DOI: 10.1002/polb.20957
20. Ray SS, Okamoto M. Biodegradable polylactide and its nanocomposites: Opening a new dimension for plastics and composites. *Macromolecular Rapid Communications* 2003;24:815-840. DOI: 10.1002/marc.200300008
21. Bhardwaj R, Mohanty AK. Advances in the properties of polylactides based materials: A review. *Journal of Biobased Materials and Bioenergy* 2007;1:197-209. DOI: 10.1166/jbmb.2007.023
22. Danley RL, Caulfield P, Aubuchon S. A rapid-scanning differential scanning calorimeter. *American Laboratory* 2008;40:9-11.
23 Mathot V, Pyda M, Pijpers T, Vanden Poel G, van de Kerkhof E,Van Herwaarden S, Van Herwaarden F, Leenaers A. The Flash DSC 1, a power compensation twin-type, chip-based fast scanning calorimeter (FSC): First findings on polymers. *Thermochimica Acta* 2011;522:36-45. DOI: 10.1016/j.tca.2011.02.031
24. Yasuniwa M, Tsubakihara S, Sugimoto Y, Nakafuku C. Thermal analysis of the double-melting behavior of poly(L-lactic acid). *Journal of Polymer Science Part B: Polymer Physics* 2004; 42:25-32. DOI: 10.1002/polb.10674
25. Di Lorenzo ML. iPP based nanocomposites filled with calcium carbonate nanoparticles: Structure/properties relationships. *Macromolecular Symposia* 2006;234:176-183. DOI: 10.1002/masy.200650220
26. Pan P, Kai W, Zhu B, Dong T, Inoue Y. Polymorphous crystallization and multiple melting behavior of Poly(L-lactide): Molecular weight dependence. *Macromolecules* 2007;40:6898-6905. DOI: 10.1021/ma071258d
27 Pan P, Zhu B, Kai W, Dong T, Inoue Y. Polymorphic transition in disordered poly(L-lactide) crystals induced by annealing at elevated temperatures. *Macromolecules* 2008;41:4296-4304. DOI: 10.1021/ma800343g

28. Yasuniwa M, Sakamo K, Ono Y, Kawahara W. Melting behavior of poly(L-lactic acid): X-ray and DSC analyses of the melting process. *Polymer* 2008;49:1943-1951. DOI: 10.1016/j.polymer.2008.02.034
29. Itaxaso Calafel M, Remiro PM, Cortazar MM, Calahorra ME. Cold crystallization and multiple melting behavior of poly(l-lactide) in homogeneous and in multiphasic epoxy blends. *Colloid and Polymer Science* 2010; 288: 283-296. DOI: 10.1007/s00396-009-2156-3
30. Shieh YT, Liu GL. Temperature-modulated differential scanning calorimetry studies on the origin of double melting peaks in isothermally melt-crystallized poly(L-lactic acid). *Journal of Polymer Science Part B: Polymer Physics* 2007; 45:466-474. DOI: 10.1002/polb.21056
31. Strobl G. Crystallization and melting of bulk polymers: New observations, conclusions and a thermodynamic scheme. *Progress in Polymer Science* 2006;31:398-442. DOI: 10.1016/j.progpolymsci.2006.01.001
32. Cheng SZD, Cao MY, Wunderlich B. Glass transition and melting behavior of Poly (Oxy-1,4-Phenyleneoxy-1,4-Phenylenecarbonyl-1,4-Phenylene). *Macromolecules* 1986;19:1868-1876. DOI: 10.1021/ma00161a015
33 Lee Y, Porter RS. Double melting behavior of poly (ether ether ketone). *Macromolecules* 1987**;**20:1336-1341. DOI: 10.1021/ma00172a028
34. Bassett DC, Olley RH, Raheil IAM. On crystallization phenomenon in PEEK. *Polymer* 1988;29:1745-1754. DOI: 10.1016/0032-3861(88)90386-2
35. Kruger KN, Zachmann HG. Investigation of the melting behavior of Poly (Aryl Ether Ketones) by simultaneous measurements of SAXS and WAXS employing synchrotron radiation. *Macromolecules* 1993;26:5202-5208.
36. Song M. Rigid amorphous phase and low temperature melting endotherm of poly(ethylene terephthalate) studied by modulated differential scanning calorimetry. *Journal of Applied Polymer Science* 2001**;**81:2779-2785. DOI: 10.1002/app.1724
37. Righetti MC, Di Lorenzo ML, Tombari E, Angiuli M. The low-temperature endotherm in poly(ethylene terephthalate): Partial melting and rigid amorphous fraction mobilization. *J Phys Chem B* 2008;112:4233-4241. DOI: 10.1021/jp076399w
38. Hoffman JD, Weeks JJ. Rate of Spherulitic Crystallization with Chain Folds in Polychlorotrifluoroethylene. *Journal of Chemical Physics* 1962;37:1723.
39. Marand H, Xu J, Srinivas S. Determination of the equilibrium melting temperature of polymer crystals: Linear and nonlinear Hoffman-Weeks extrapolations. *Macromolecules* 1998;31:8219-8829. DOI: 10.1021/ma980747y
40. Pyda M, Bopp RC, Wunderlich B. Heat capacity of poly(lactic acid). *Journal of Chemical Thermodynamics* 2004;36:731-742. DOI: 10.1016/j.jet.2004.02.003
41. Fitzpatrick S, McCabe JF, Petts CR, Booth SW. Effect of moisture on polyvinylpyrrolidone in accelerated stability testing. *International Journal of Pharmaceutics* 2002;246:143-151. DOI: 10.1016/S0378-5173(02)00375-7
42. Zhang G, Zhang J, Zhou X, Shen D. Miscibility and phase structure of binary blends of polylactide and poly(vinylpyrrolidone). *Journal of Applied Polymer Science* 2003; 8:973-979. DOI: 10.1002/app.11735
43. Fornes TD, Paul DR. Crystallization behavior of nylon 6 nanocomposites. *Polymer* 2003;44:3945-3961. DOI: 10.1016/S0032-3861(03)00344-6
44. Moynihan CT, Easteal AJ, DeBolt MA, Tucker J. Dependence of the Fictive Temperature of Glass on Cooling Rate. *Journal of American Ceramic Society* 1976;59:12-16.

45. Zereshki S, Figoli A, Madaeni SS, Simone S, Jansen JC, Esmailinezhad M, Drioli E. Poly(lactic acid)/poly(vinyl pyrrolidone) blend membranes: Effect of membrane composition on pervaporation separation of ethanol/cyclohexane mixture. *Journal of Membrane Science* 2010; 362: 105-112. DOI: 10.1016/j.memsci.2010.06.025
46. Woo T, Halley P, Martin D, Kim DS. Effect of different preparation routes on the structure and properties of rigid polyurethane-layered silicate nanocomposites. *Journal of Applied Polymer Science* 2006;102:2894-2903. DOI: 10.1002/app.24787

Table 1: Composition of nanocomposites produced by electrospinning

Clay loading in electrospinning solution (wt. %)	**PLA wt. % in solution**	**PVP wt. % in solution**	**Clay/PLA Ratio**	**Clay loading in nanocomposite (wt. %)**	**PVP loading in nanocomposite (wt. %)**
0	10	0	0	0	0
2	10	1	0.2	15.3	7.6
4	10	2	0.4	25.0	12.5

Figures

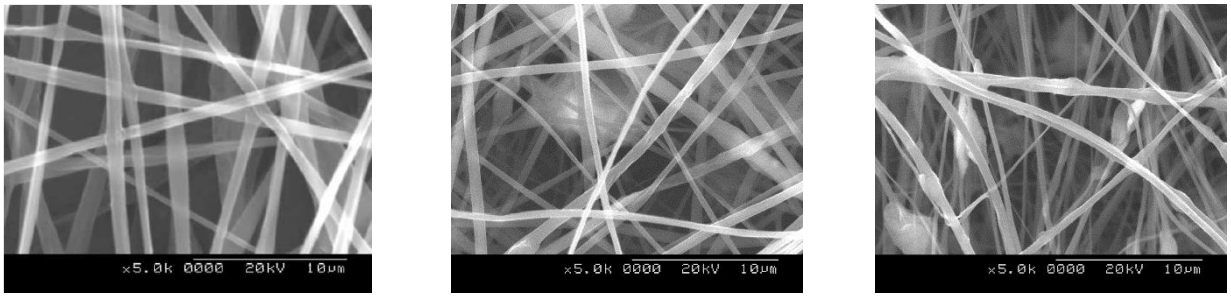

a) b) c)

Figure 1: SEM images of electrospun fiber mats (a) neat PLA b) 15.3 wt. % clay c) 25.0 wt.% clay

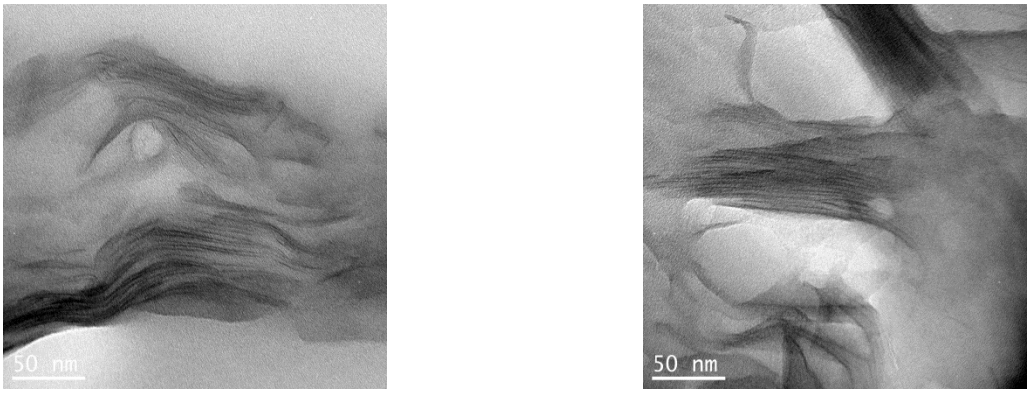

a) b)

Figure 2: TEM images of cross sections for a) 15.3 wt. % clay sample b) 25.0 wt. % clay sample

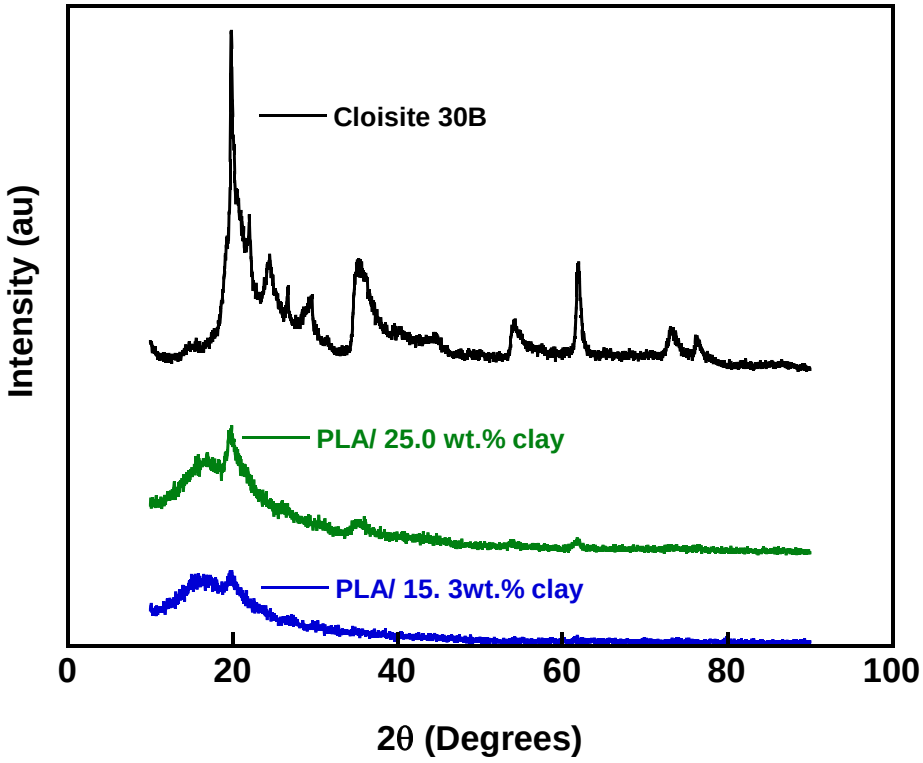

Figure 3: XRD spectra of neat PLA compared with PLA/clay nanocomposites

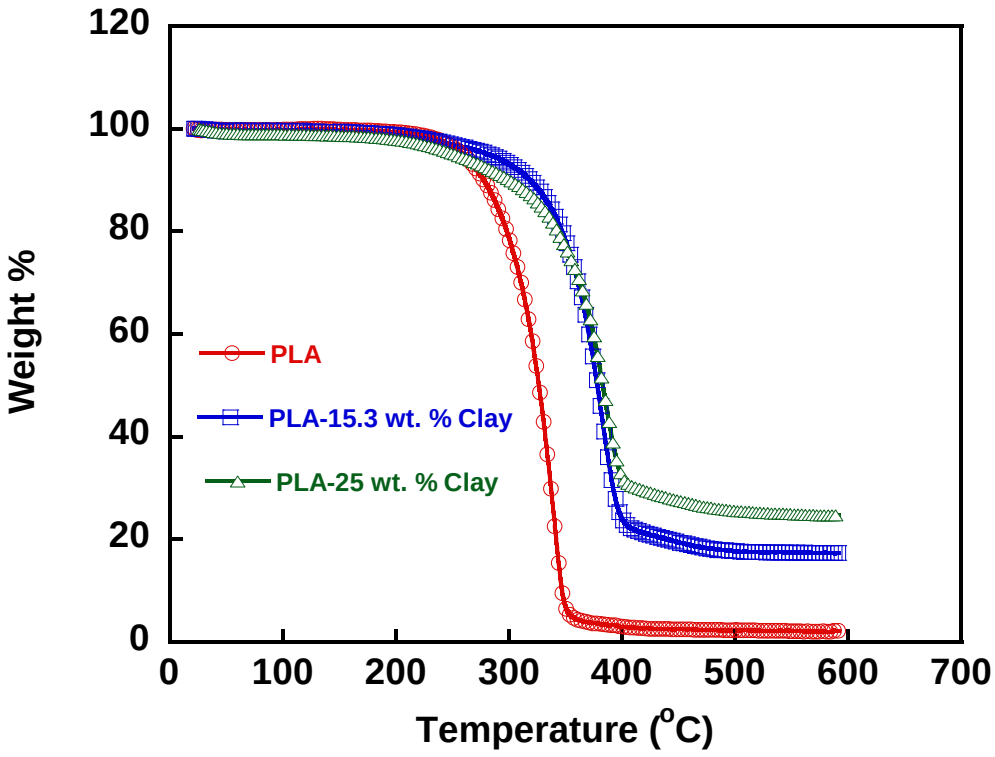

Figure 4: TGA curves of PLA and PLA/clay nanocomposites with different clay loadings.

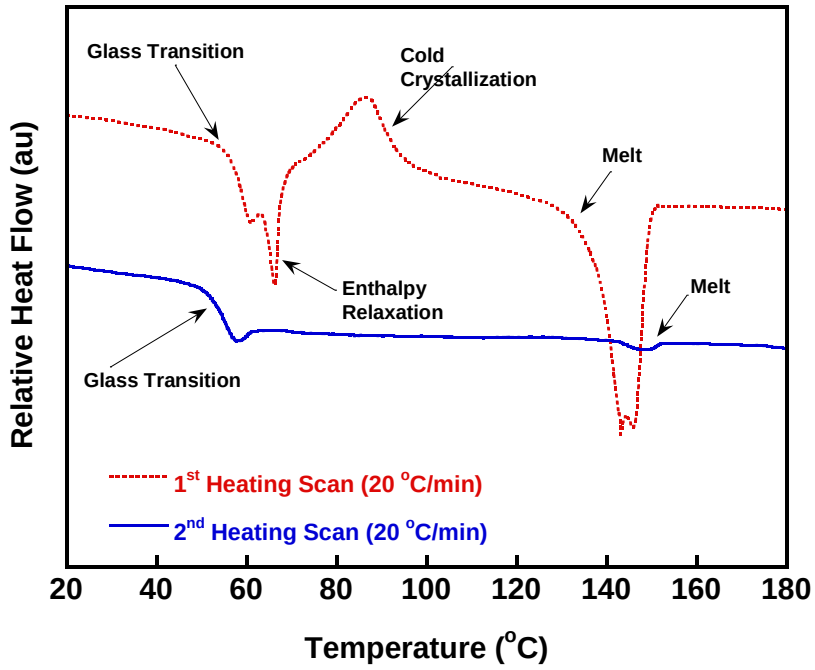

a)

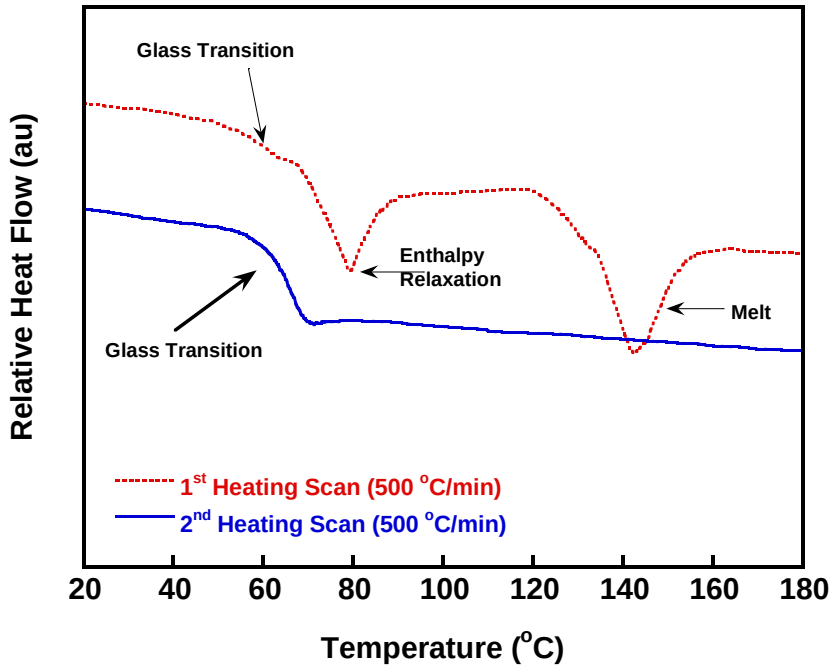

b)

Figure 5: A comparison of heat flow curves obtained on a) heating the as-prepared neat PLA sample at 20 °C/min (1st heating scan) and heating at 20 °C/min following cooling from the melt at 20 °C/min (2nd heating scan); b) Heating the as-prepared neat PLA sample at 500 °C/min (1st heating scan) and heating at 500 °C/min following cooling from the melt at 500 °C/min (2nd heating scan).

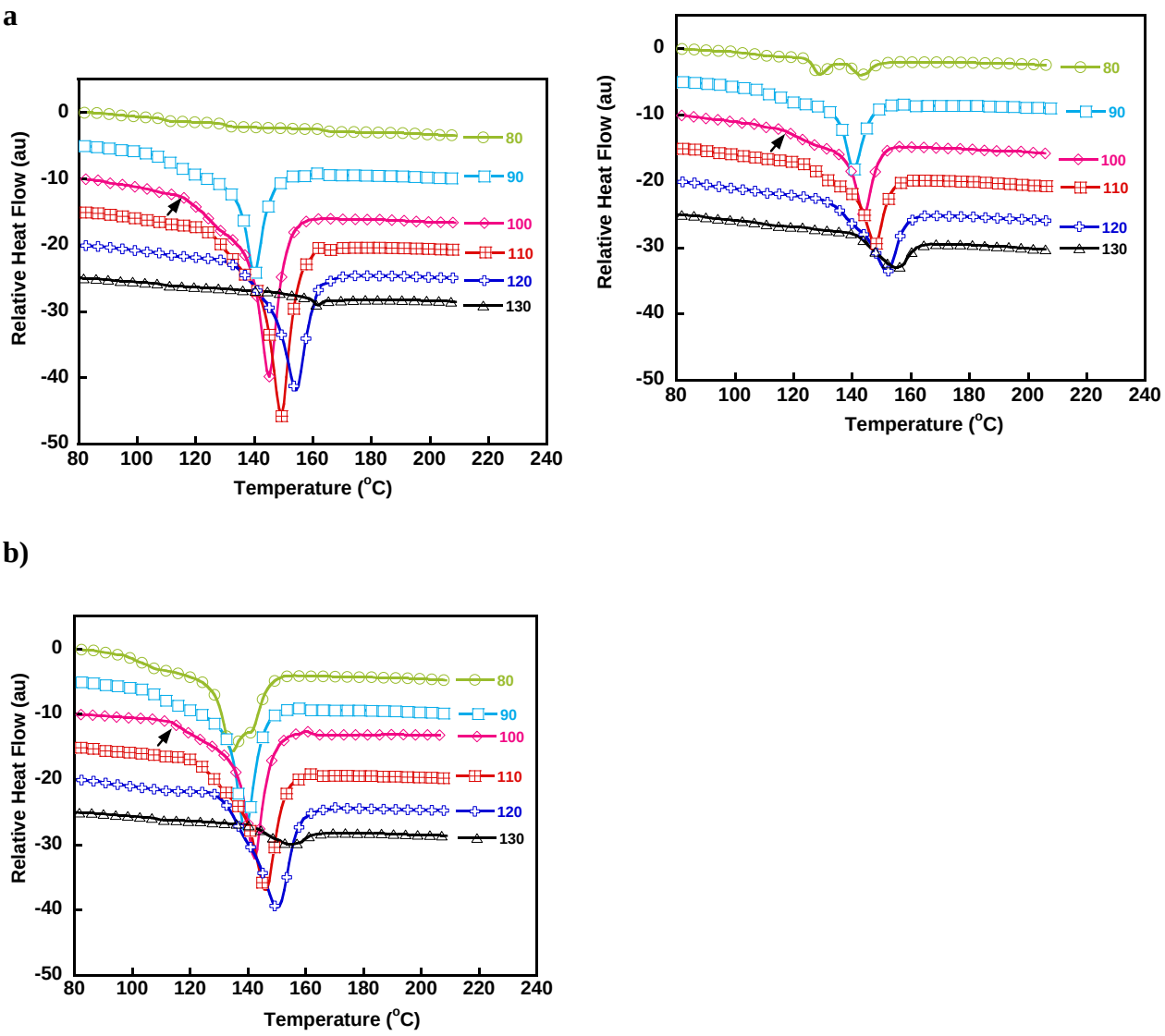

Figure 6: Heat flow curves obtained on heating at 500 °C/min following isothermal melt crystallization at various temperatures for 60 minutes for a) neat PLA b) 15.3 wt. % clay c) 25.0 wt. % clay.

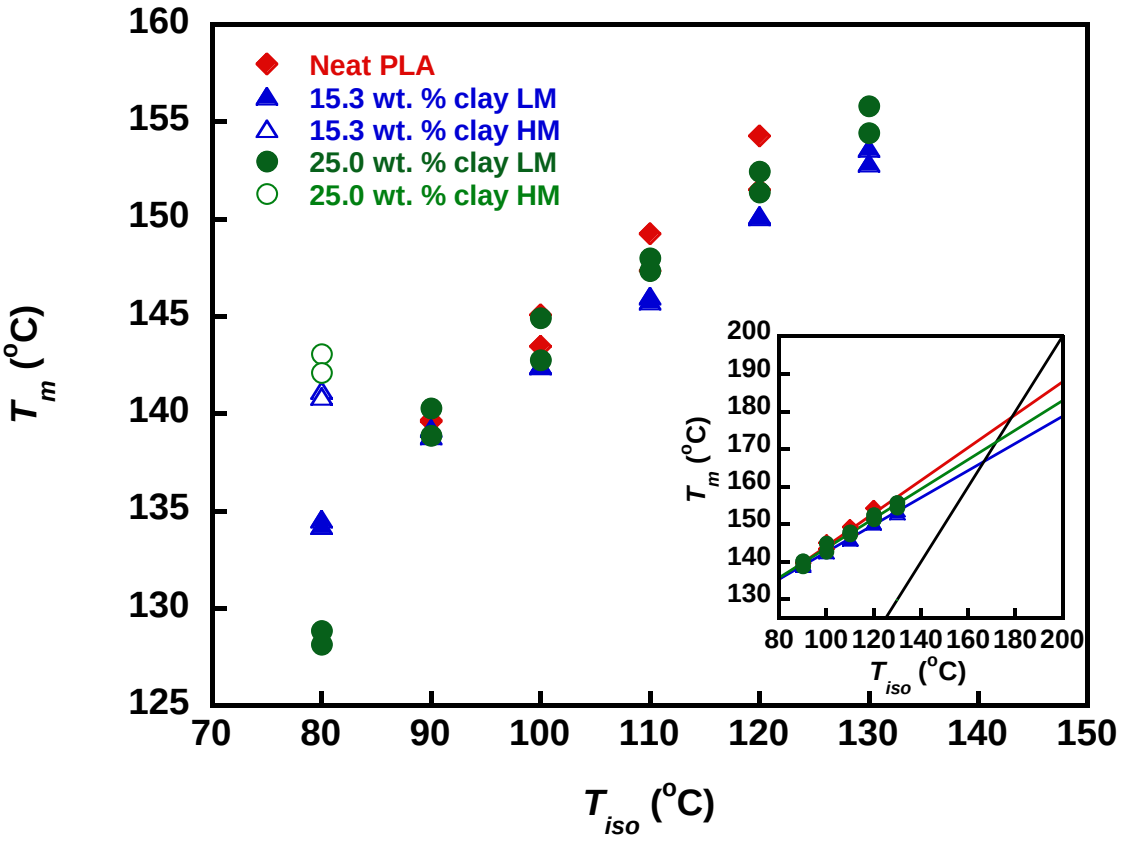

Figure 7: Relationship between T_m and T_{iso} for PLA and PLA/clay nanocomposites. The letters LM and HM represent the peak temperatures of the low and high temperature endotherms, respectively. The result of Hoffman Weeks method for the determination of T_m^0 is shown in the inset.

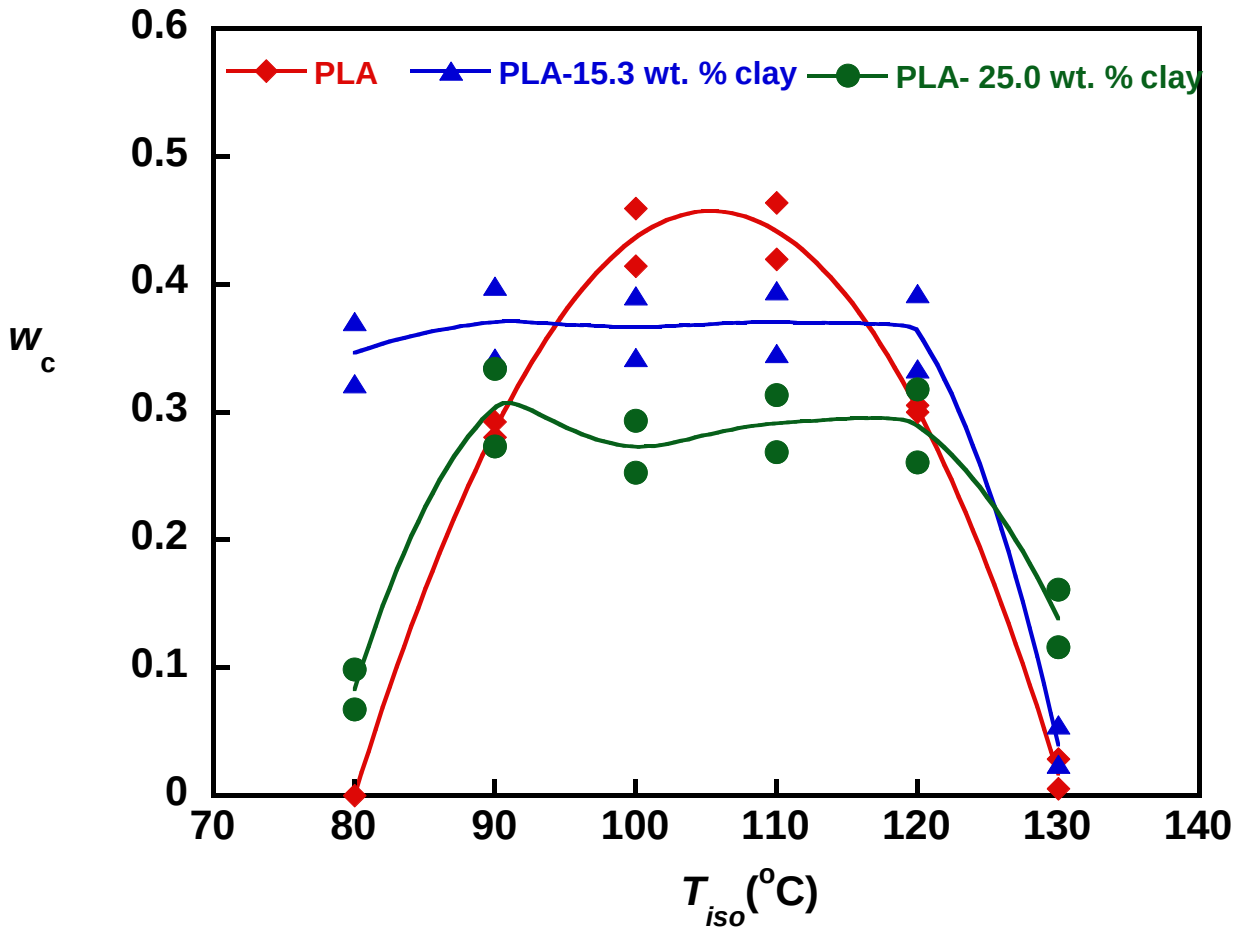

Figure 8: A comparison of crystallinity for PLA and PLA/clay nanocomposites obtained on heating at 500 °C/min following isothermal melt crystallization at various values of T_{iso} for 60 min. Lines are drawn as a visual guide. Two specimens were characterized at each T_{iso} for all three sample types (i.e., 0 wt. % clay, 15.3 wt. % clay, and 25.0 wt.% clay).

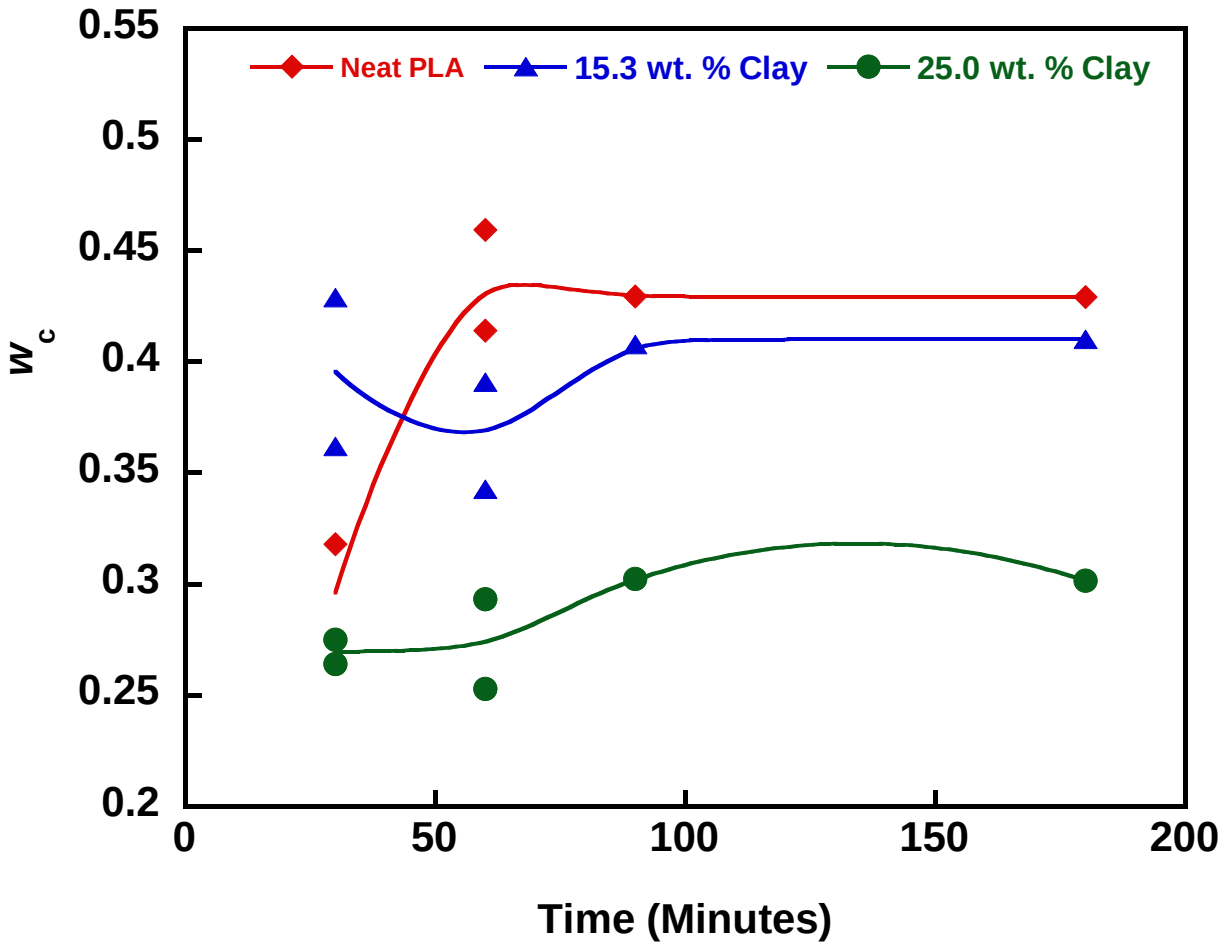

Figure 9: A comparison of crystallinity for PLA and PLA/clay nanocomposites obtained on heating at 500 °C/min following isothermal melt crystallization at T_{iso} = 100 °C for various periods from 30 to 180 min. Two specimens were characterized at isothermal periods of 30 min for all three sample types. For isothermal periods longer than 60 min, no change in w_c was observed and only one measurement was performed.

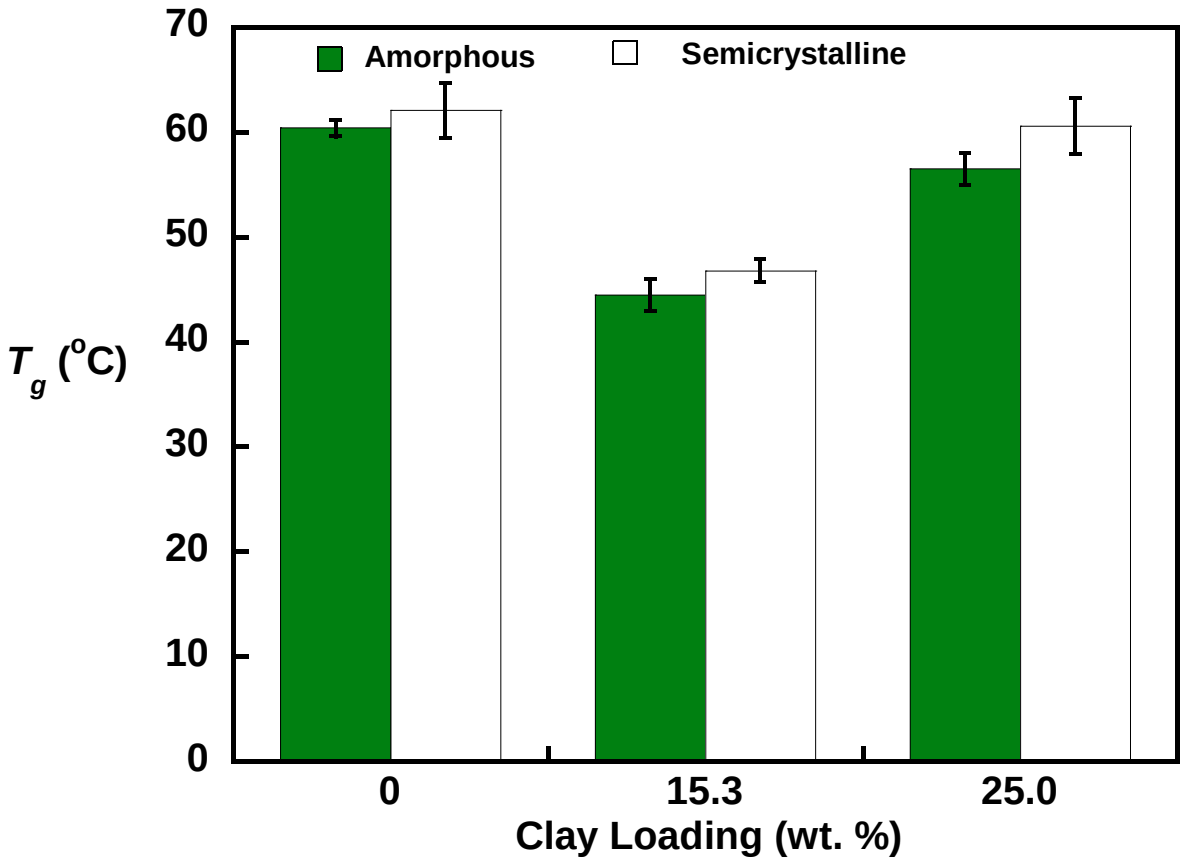

Figure 10: Effect of clay loading on glass transition temperature (T_g) of PLA and PLA/clay nanocomposites. The values for amorphous T_gs were obtained based on three measurements for each sample. The values of semicrystalline T_gs were based on four measurements at 100 °C , following complete crystallization. The error bars represent standard deviations of the measurements.